Vehicle System Dynamics
International Journal of Vehicle Mechanics and Mobility

ISSN: 0042-3114 (Print) 1744-5159 (Online) Journal homepage: www.tandfonline.com/journals/nvsd20

Improving the stability of high-speed trains using an innovative passive yaw damper

Xiangwang Chen, Yan Zhou, Yuan Yao & Ton van Dongen

VEHICLE SYSTEM DYNAMICS
2026, VOL. 64, NO. 1, 226–249
https://doi.org/10.1080/00423114.2024.2427749

Improving the stability of high-speed trains using an innovative passive yaw damper

Xiangwang Chen[a,b], Yan Zhou[a], Yuan Yao [a,b] and Ton van Dongen[c]

[a]State Key Laboratory of Rail Transit Vehicle System, Southwest Jiaotong University, Chengdu, People's Republic of China; [b]The State Key Laboratory of Heavy-duty and Express High-power Electric Locomotive, CRRC Zhuzhou Electric Locomotive Co., Ltd., Zhuzhou, People's Republic of China; [c]KONI BV, Oud-Beijerland, Netherlands

ABSTRACT

Ensuring lateral stability is essential for achieving excellent operation safety and ride comfort of high-speed trains. However, complicated operational environments, particularly various wheel-rail contact geometries, would result in the occurrence of hunting instability. This study presents an innovative passive yaw damper to improve the stability of a high-speed train undergoing extreme wheel-rail contact conicities. A sensitivity analysis of the vehicle stability is first performed to demonstrate the importance of the dynamic stiffness of yaw dampers, promoting the application of the innovative damper. Experimental characterisation procedures enable the detailed investigation into the static and dynamic characteristics of the innovative damper, which are compared with those of conventional passive dampers to highlight the difference. To simulate the dynamic behaviour of the yaw damper, a numerical modelling method based on the Maxwell model is proposed. Using this method, the effectiveness of the innovative damper is assessed in terms of improving the vehicle stability at various wheel-rail conicities. The results show that the innovative yaw damper can ensure carbody stability at low conicity and bogie stability at high conicity, superior to conventional dampers, which fail to balance the vehicle stability at distinct conicities and usually result in hunting instability in specific wheel-rail contact states.

ARTICLE HISTORY
Received 7 May 2024
Revised 10 October 2024
Accepted 5 November 2024

KEYWORDS
Stability; yaw damper; dynamic stiffness; high-speed train; sensitivity analysis

1. Introduction

Hunting instability may occur during the long-term service of high-speed trains due to complicated operational conditions, resulting in a range of issues threatening the regular operation, such as deterioration of ride comfort, damage to wheels and rails, and even derailment. It is a self-excited motion inherent in railway vehicles and is characterised by the sustained lateral and yaw motion of wheelsets, bogies, or the whole vehicle. According to the vibration characteristics, hunting instability can be divided into two distinct forms: carbody hunting and bogie hunting. The former is characterised by the presence of large-amplitude oscillations of the carbody, while the latter exhibits violent oscillations of

CONTACT Yuan Yao yyuan8848@163.com

the bogie. In most cases, these two instability forms both result from the poor wheel-rail contact relationship remarkably deviating from the designed one [1–4]. Consequently, one straightforward way to deal with hunting instability is timely wheel reprofiling and rail grinding [5], which, however, increases operation and maintenance costs and reduces the availability of vehicles. Another effective alternative solution is to optimise suspension parameters [6–9], among which the parameters of yaw dampers are generally selected carefully due to their notable influence on the running dynamics of vehicles. The yaw damper installed longitudinally between the carbody and bogie frame aims to suppress the tendency towards hunting and increase the vehicle's critical speed. Its performance degradation would cause serious vehicle instability problems [10,11]. Extensive research work [12–16] has focused on the influence of yaw damper parameters on the dynamic performance of railway vehicles through theoretical and experimental methods so as to provide guidelines on selecting appropriate types of yaw dampers.

However, numerous studies revealed that different aspects of vehicle dynamic performance have distinct requirements for yaw damper parameters, and the parameter determination of conventional passive yaw dampers has to make a compromise. To further improve the dynamic performance, the active yaw damper was designed and tested [17–19]. It can adjust the vehicle's behaviour to varied track features. The active yaw damper was proposed mainly to solve the trade-off between vehicle stability and curving performance, and more recently, Shi et al. [20,21] have utilised it to improve the vehicle stability in extreme wheel conicity cases and investigated the bifurcation behaviour of the vehicle under active yaw control. However, the high complexity and costs, as well as concerns about the failure inhibit the commercial application of the active yaw damper. For this reason, Wang et al. [22] introduced a hydraulic semi-active yaw damper as a compromise alternative for the improvement of the bogie stability of a high-speed rail vehicle and validated its effectiveness through numerical simulations. Zhang et al. [23] adopted an eddy current damper with the parallel inerter as the yaw damper to improve the lateral dynamic performance of high-speed trains in extreme wheel-rail contact states. The optimal parameter configuration is proposed by the muti-objective optimisation concerning the lateral ride comfort and linear stability.

Compared with full-active and semi-active technologies, some innovative passive suspensions with special components can also provide similar functions to improve vehicle performance. However, they significantly reduce the design complexity and maintenance costs and avoid the potential adverse effects introduced by degraded control reliability. The position dependent yaw damper [24] and frequency-selective damping yaw damper [25] have proven to enhance the curving performance of high-speed railway vehicles without reducing their high-speed stability. These innovative dampers reduce the output force when the vehicle negotiates sharp curves, on which the internal special structures take effect once the amplitude or frequency of the damper stroke overcomes a designed threshold. Besides, the frequency-selective damping damper was also ultilised to deal with the trade-off between carbody stability and bogie stability of a high-speed locomotive [26]. Based on the parameter influencing analysis, Yao et al. [27] proposed to replace conventional rubber joints with hydraulic bushings at the ends of the yaw damper for desired frequency-dependent stiffness of the damper, which can achieve the robust lateral stability of high-speed trains according to the preliminary analysis results.

This study focuses on an innovative passive damper, called frequency-selective stiffness (FSS) yaw damper, which realises the stiffness modification by incorporating a new valve component patented by Koni BV. Huo et al. [28] have introduced this damper to enhance the stability of a high-speed passenger car. Unfortunately, the dynamic characteristics of the damper were solely investigated at a certain excitation amplitude. Besides, its effect on the dynamic performance of high-speed trains concentrated on the low wheel-rail conicity condition, obtaining the wheelset displacement response through the roller rig test. As a supplement, this study extends the research on the FSS yaw damper from the perspective of numerical simulations by proposing a parameter determination procedure for a non-linear damper model. This model is adopted to detail the effect of the FSS damper on the vehicle dynamic performance under various operational conditions which are difficult to reproduce on the roller rig test bench. This study aims to obtain the detailed characteristics of the FSS damper and carry out its application evaluation, thereby laying the foundations for the damper performance optimisation and subsequent engineering applications.

This paper is structured as follows. Section 2 performs a sensitivity analysis on the stability of a high-speed railway vehicle to demonstrate the importance of yaw damper parameters, especially its dynamic stiffness, which supports the application of the FSS damper in the improvement of vehicle stability. Section 3 introduces the main structure of the FSS damper and its measurements of static and dynamic characteristics. A numerical modelling method for the yaw damper is presented as well. It successfully reproduces the behaviour of the yaw damper and is suitable for vehicle dynamics simulations. Section 4 investigates the effect of the FSS damper on the vehicle stability under extreme wheel-rail contact conditions by comparing its resulting vehicle dynamic responses with those obtained by conventional passive dampers. Finally, conclusions are obtained in Section 5.

2. Sensitivity analysis of vehicle stability

2.1. Vehicle dynamic model

A multibody dynamic model of a high-speed rail vehicle is developed in the commercial software SIMPACK based on its actual parameters. It consists of one carbody, two bogie frames, four wheelsets, and eight axle boxes, with a total of 50 degrees of freedom. The vehicle has two stages of suspensions. The primary suspension consists of axle box springs, trailing arm rubber joints, and vertical dampers. The secondary suspension includes air springs, lateral dampers, vertical dampers, yaw dampers, anti-roll bars, and lateral bump stops. Each side of a bogie is equipped with two parallel yaw dampers. These suspension components are modelled by linear and nonlinear spring and dashpot elements, among which the Maxwell model composed of a spring in series of a dashpot is used to represent the dampers, whose nonlinear damping characteristics are fully considered.

The wheel-rail interaction is based on the wheel profile S1002CN and rail profile CHN60, considering a rail cant of 1:40 and a standard gauge of 1435 mm. The Hertz theory is used to solve the normal contact problem, while the FASTSIM algorithm is applied to calculate the creep force. The friction coefficient in the wheel-rail interface is set to 0.35. Additionally, the track irregularities measured from the Wuhan-Guangzhou mainline are adopted in the following dynamics simulations.

2.2. Evaluation method of stability

Carbody hunting is characterised by the severe carbody swaying with a low frequency to which the human body is sensitive, significantly worsening the ride comfort of passengers.

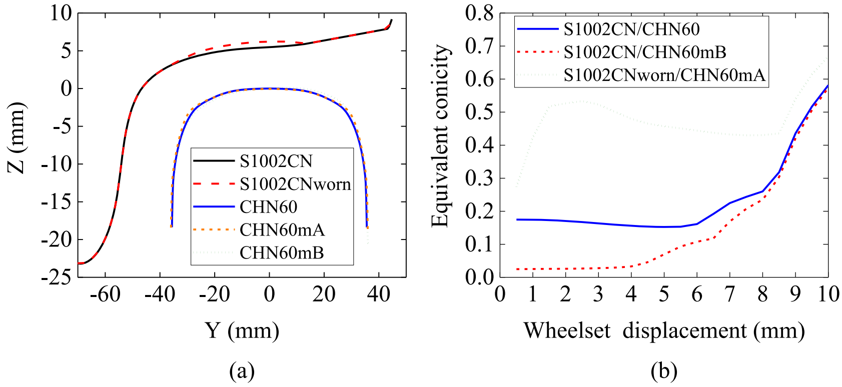

Figure 1. Wheel-rail contact geometries: (a) wheel-rail profiles; (b) wheel-rail contact equivalent conicity.

It has been widely recognised that a low wheel-rail contact conicity is the principal cause of carbody hunting [1,2]. Therefore, adopting the combination of a standard wheel profile S1002CN and a measured rail profile CHN60mB, as shown in Figure 1(a), this study investigates the carbody stability of the high-speed vehicle under a low-conicity condition. The equivalent conicity at 3 mm wheelset lateral displacement is 0.03, much lower than that obtained from the standard profile combination S1002CN/CHN60. The Sperling index W calculated from the measurement of carbody vibration acceleration is widely used to evaluate the ride comfort and is defined as follows [29]

$$W = 3.57 \sqrt[10]{\frac{A^3}{f} F(f)} \tag{1}$$

where A is the acceleration amplitude in the frequency domain (Unit: m/s^2), f is the corresponding frequency (Unit: Hz), and $F(f)$ is the frequency correction function. For passenger vehicles, the limit values of ride comfort are defined as 2.5, 2.75 and 3.0 for excellent, medium and qualified levels, respectively. In general, the excellent level is required during vehicle operation.

Conversely, bogie hunting manifests as the violent high-frequency vibration of the bogie and may give rise to derailment. It usually occurs when the equivalent conicity is too high [3,4]. In this study, the bogie stability of the vehicle is evaluated using a worn wheel profile S1002CNworn and a measured rail profile CHN60 mA. As depicted in Figure 1(b), this profile combination results in a high equivalent conicity of 0.52. There are various methods for assessing bogie stability . We adopt the simplified measuring method defined in EN 14363:2016 [30], which uses the lateral bogie frame acceleration measured above the axle box. The acceleration signal is first processed by a bandpass filter with a pass band $f_0 \pm 2$ Hz, where f_0 refers to the dominant frequency of the unstable bogie motion. Then the sliding root mean square (RMS) of the filtered signal is computed over a 100 m window length with steps of 10 m. The maximum value A_{high} of the sliding RMS values is selected as the evaluation index and should be compared with the limit value $\ddot{y}^{+}_{\mathrm{lim}}$ defined as follows.

$$\ddot{y}^{+}_{\mathrm{lim}} = \frac{1}{2}\left(12 - \frac{m_{\mathrm{b}}}{5}\right) = 5.32 \text{ m/s}^2 \tag{2}$$

where m_{b} denotes the bogie mass in tons.

Table 1. Evaluation indexes of the vehicle stability.

Index	Speed (km/h)	Equivalent conicity	Description
W_{low}	250	0.03	Evaluation index for carbody stability
A_{high}	400	0.52	Evaluation index for bogie stability

Table 1 summarises the stability indexes and their simulation scenarios. The ride comfort index W_{low} is calculated at a running speed of 250 km/h, given that carbody hunting is usually more severe at a relatively low speed. On the contrary, bogie hunting would intensify as the running speed increases, so A_{high} is calculated at a high speed of 400 km/h. All dynamics simulations are performed on tangent tracks.

2.3. Global sensitivity analysis

Global sensitivity analysis can quantify the contributions of different input variables to the variability of objective functions [31], playing an important role in reducing the number of design variables and improving the computational efficiency in parameter design. The Sobol sensitivity analysis method [32] is adopted here for its ability to address nonlinear model responses and obtain robust analysis results. This method is a Monte Carlo method based on variance decomposition.

The objective function $f(x)$ can be decomposed into the sum of 2^n terms:

$$f(x) = f_0 + \sum_{i=1}^{n} f_i(x_i) + \sum_{1<i<j\leq n}^{n} f_{ij}(x_i, x_j) + \ldots + f_{12\cdots n}(x_1, x_2, \cdots, x_n) \tag{3}$$

where f_0 is a constant, x_i, x_j are the different input variables whose values are normalised into the unit interval [0, 1], and n is the total number of variables. If the function components in Equation (3) are orthogonal and can be expressed as integrals of $f(x)$, then the total variance D of $f(x)$ and variance $D_{i_1\cdots i_s}$ of $f_{i_1\cdots i_s}$ can be obtained by squaring Equation (3) and integrating over the unit interval:

$$D = \int f^2(x)dx_1dx_2\cdots dx_n - f_0^2 \tag{4}$$

$$D_{i_1\cdots i_s} = \int f_{i_1\cdots i_s}^2 dx_{i_1}\cdots dx_{i_s} \tag{5}$$

where $1 \leq i_1 < \cdots < i_s \leq n$. The global sensitivity index is defined as follows:

$$S_{i_1\cdots i_s} = \frac{D_{i_1\cdots i_s}}{D} \tag{6}$$

The variance $D_{\boldsymbol{X}_1}$ and global sensitivity index $S_{\boldsymbol{X}_1}$ corresponding to a variable subset $\boldsymbol{X}_1 = [x_{k_1}, x_{k_2}, \cdots, x_{k_z}]^{\text{T}}$ can be obtained similarly:

$$D_{\boldsymbol{X}_1} = \sum_{s=1}^{z} \sum_{(i_1<\cdots<i_s)\in K} D_{i_1\cdots i_s} \tag{7}$$

$$S_{\boldsymbol{X}_1} = \frac{D_{\boldsymbol{X}_1}}{D} \tag{8}$$

Table 2. Sampling ranges of the suspension parameters.

Parameters	Sampling ranges	Description
K_{px}	10–120 (kN/mm)	Primary longitudinal stiffness
K_{py}	3–20 (kN/mm)	Primary lateral stiffness
C_{yd}	200–2000 (kN·s/m)	Dynamic damping of the yaw damper
K_{yd}	3–20 (kN/mm)	Dynamic stiffness of the yaw damper
C_{sy}	10–60 (kN·s/m)	Secondary lateral damping

where $K = [k_1, k_2, \dots, k_z]$. Assuming that $\mathbf{X}_2$ is the complementary subset of $\mathbf{X}_1$, the total variance $D^{\mathrm{T}}_{\boldsymbol{X}_2}$ and sensitivity index $S^{\mathrm{T}}_{\boldsymbol{X}_2}$ of $\mathbf{X}_2$ are defined as follows:

$$D^{\mathrm{T}}_{\boldsymbol{X}_2} = D - D_{\boldsymbol{X}_1} \tag{9}$$

$$S^{\mathrm{T}}_{\boldsymbol{X}_2} = \frac{D^{\mathrm{T}}_{\boldsymbol{X}_2}}{D} \tag{10}$$

The total sensitivity index reflects the total influence of an input variable on the objective function, including all the possible interactions between that variable and the others.

Calculating the sensitivity index requires the high-dimensional integrals of objective functions, which results in a heavy computational burden and would be a tough task for complex nonlinear systems such as rail vehicles. Therefore, this study establishes the surrogate model employing the Support Vector Regression (SVR) with a radial kernel function to describe the mapping relationship between suspension parameters and stability indexes. SVR is based on the structural risk minimisation principle and can accurately represent the high-dimensional function [33]. As an efficient stratified random sampling method, the Latin Hypercube Sampling (LHS) is used to collect 300 samples for the construction of the surrogate model. The investigated suspension parameters are those closely related to the lateral dynamic performance of high-speed trains, including primary longitudinal stiffness K_{px}, primary lateral stiffness K_{py}, dynamic damping C_{yd} (series damping in the Maxwell model) of the yaw damper, dynamic stiffness K_{yd} (series stiffness in the Maxwell model) of the yaw damper, and secondary lateral damping C_{sy}. Their sampling ranges are presented in Table 2 on the basis of the current values adopted in different types of high-speed trains in China.

Using the established SVR surrogate model, Figure 2(a) displays the total sensitivity indexes of stability indexes W_{low} and A_{high} with respect to each suspension parameter. The sensitivity index is positive, and a higher value indicates a more significant influence on the vehicle stability. It can be drawn that W_{low} is sensitive to K_{px}, C_{yd}, K_{yd}, and C_{sy}, with K_{yd} demonstrating the most significant effect on the carbody stability at low conicity. A_{high} is also highly sensitive to K_{yd} while insensitive to the other suspension parameters. Hence, the value of K_{yd} must be carefully determined considering its great importance on the vehicle stability. Its slight change may result in a remarkable variation in the stability indexes.

While the sensitivity index can quantify the considerable contribution of K_{yd} to the vehicle stability, it cannot reveal their variation trends depending on each other. To this end, the sampling results of LHS are shown in Figure 2(b), where linear regression is also applied to clearly describe the relationship between K_{yd} and stability indexes. It

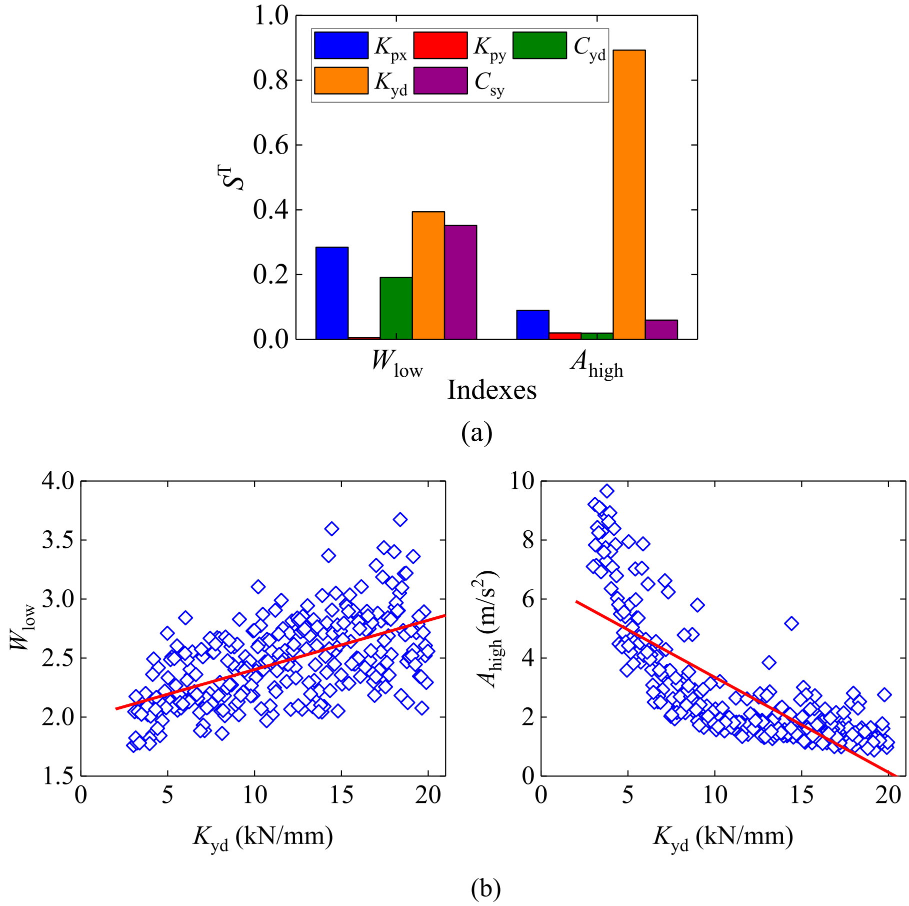

Figure 2. Global sensitivity analysis results: (a) total sensitivity indexes; (b) relationship between K_{yd} and stability indexes in Latin hypercube sampling.

can be observed that W_{low} increases with K_{yd} on average, while A_{high} decreases as K_{yd} increases. There are distinct requirements for the value of K_{yd} to ensure carbody stability at low conicity and bogie stability at high conicity. According to the frequency characteristics of carbody hunting and bogie hunting, the desired dynamic stiffness of the yaw damper should behave as a low value at low frequencies and a high value at high frequencies, namely significant frequency-dependent stiffness. However, conventional yaw dampers have limited frequency-dependent characteristics and thus fail to achieve excellent stability of high-speed trains subjected to complicated wheel-rail contact relationships.

3. Damper characterisation and modelling

3.1. Structure and characteristic of the FSS yaw damper

In order to realise the desired frequency-dependent dynamic stiffness, this paper investigates the innovative FSS yaw damper in detail.

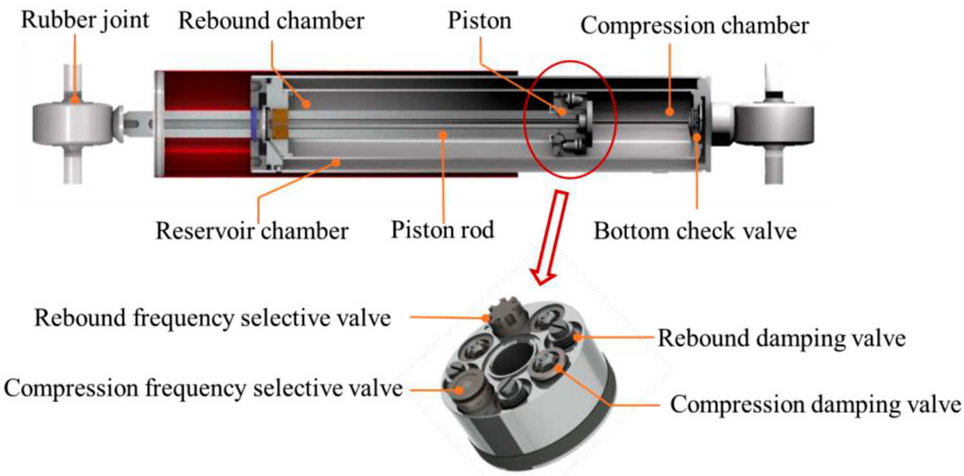

Figure 3. Structure sketch of the FSS yaw damper.

Figure 3 displays the structure sketch of the FSS damper. Like conventional yaw dampers, it is mainly composed of the piston rod, piston, rebound chamber, compression chamber, reservoir chamber, damping valve, bottom check valve, and rubber joint. Besides, the FSS yaw damper introduces a pair of additional FSS valves on the piston, which makes it exhibit different characteristics. The FSS valves work together with three pairs of damping valves on the piston to provide the damping force. Specifically, during the compression or rebound stroke of the yaw damper, three corresponding damping valves and one FSS valve take effect. Since the damping force is produced by the pressure difference between the compression chamber and rebound chamber below and above the piston, the compression and rebound chambers are also called working chambers. They communicate with each other through the valves installed on the piston. After introducing the FSS valves, the yaw damper will show different oil flow and pressure drop from the standard one between the working chambers, leading to a significant change in the damping force when subjected to the same displacement excitation. The FSS valve has a delicate internal structure, including spring, constant orifice, auxiliary piston, and so on. To obtain the desired dynamic characteristics of the yaw damper, these structural parameters should be carefully designed and achieve a reasonable match with those of the damping valves.

To investigate the characteristics of the FSS yaw damper, a series of tests with diverse excitation inputs are carried out on a dedicated test bench equipped with an electro-hydraulic servo system. During the test, the clamps fix the yaw damper at its nominal instalment length. A controlled sinusoidal displacement excitation with varied amplitudes and frequencies is imposed on the end of the yaw damper, while a load cell measures the actual force provided by the device. For each case, five complete cycles are performed, and the data from the last cycle is adopted to describe the characteristics of the damper. Moreover, to highlight the characteristics introduced by the FSS technology, the measurements [34] of two different types of conventional passive yaw dampers (referred to as YD1 and YD2) are also displayed for comparison. These two conventional dampers are widely used in the high-speed train investigated in this paper but exhibit distinct characteristics.

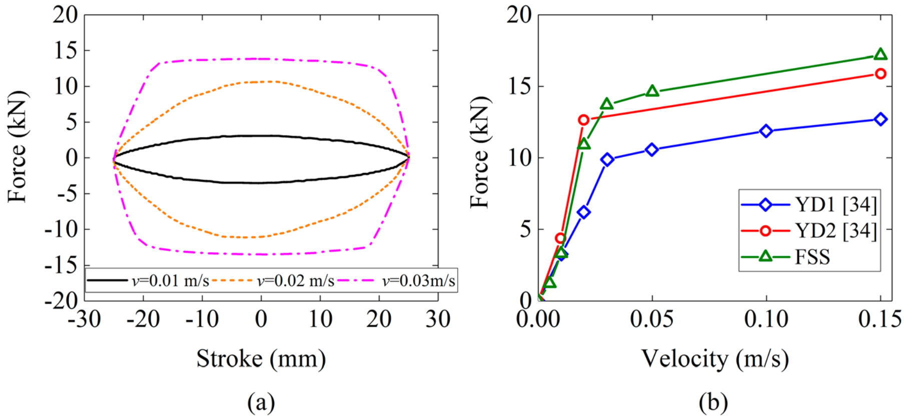

Figure 4. Static characteristics of the yaw damper: (a) measured force-displacement hysteresis curves of the FSS yaw damper; (b) comparison of the force-velocity characteristic curve between the FSS and conventional yaw dampers.

The static characteristics of the yaw damper are first obtained under displacement excitations with a large amplitude (25 mm) and different low frequencies. Figure 4(a) shows some measured force-displacement hysteresis curves of the FSS damper. The shape of the hysteresis curves is similar to that of conventional yaw dampers and exhibits favourable symmetry during compression and rebound strokes. In addition, the FSS damper blows off when the maximum velocity exceeds 0.03 m/s. Figure 4(b) compares the force-velocity characteristic curves between the FSS damper and the conventional dampers, with the damping force selected as the average of the maximum absolute values during compression and rebound strokes. Compared with two conventional dampers, the FSS damper displays a moderate force before blowing off and achieves the largest force after that. Additionally, the blow-off velocity of the FSS damper is higher than that of YD2 and close to that of YD1. On the whole, the FSS damper is similar to conventional dampers regarding the static characteristic, and no special features are found there.

The static characteristic of the yaw damper is more concerned when the vehicle operates on a tight curve, since it deforms with a large amplitude and low frequency in that case. However, high-speed trains in China generally operate on large-radius curves and straight tracks at high speeds, so it is crucial to pay attention to the dynamic characteristics of the yaw damper under small-amplitude and high-frequency displacement excitations. According to the measurements in field tests, the displacement of the yaw damper is always within a short stroke of 2 mm, even in the presence of hunting instability [35]. Therefore, harmonic excitations with an amplitude of 1 and 2 mm are applied in the dynamic characteristic test, with the excitation frequency varying from 1 Hz to 10 Hz.

Figure 5 shows the test results of the dynamic characteristics of the FSS yaw damper. It can be seen from Figure 5(a) that the shape of the measured hysteresis curves is also similar to that of conventional hydraulic dampers. The hysteresis curve is elliptical at the excitation amplitude of 1 mm. With increasing excitation frequency, the amplitude of the damping force increases significantly. At the excitation amplitude of 2 mm, the force amplitude and area surrounded by the hysteresis curve change slowly when the frequency is higher than 2 Hz, as the FSS damper has blown off.

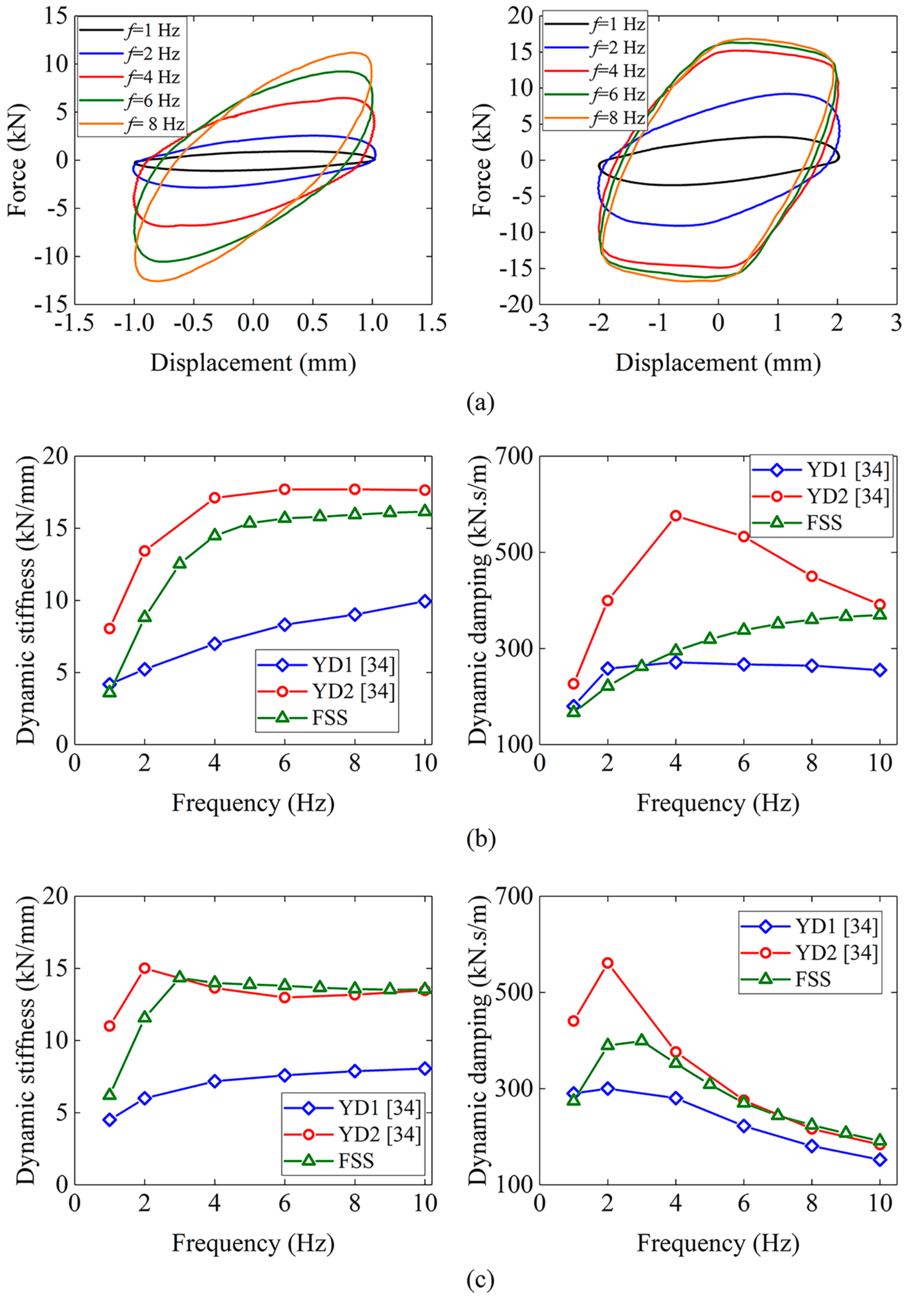

Figure 5. Dynamic characteristics of the yaw damper: (a) measured hysteresis curves of the FSS yaw damper; (b) comparison of the dynamic characteristics at excitation amplitude of 1 mm; (c) comparison of the dynamic characteristics at excitation amplitude of 2 mm.

To clearly compare the difference in dynamic characteristics of the yaw dampers, the dynamic stiffness K_{yd} and dynamic damping C_{yd} are calculated based on the hysteresis curve [36]:

$$K_{yd} = \frac{F_{reb}^{max} + F_{com}^{max}}{2d_0}\sqrt{1 + \tan^2\varphi} \tag{11}$$

$$C_{yd} = \frac{K_{yd}}{\omega \tan \varphi} \tag{12}$$

where F_{com}^{max} and F_{reb}^{max} represent the maximum absolute value of the damping force during compression and rebound stokes, respectively, d_0 is the displacement amplitude, ω is the angular frequency of the harmonic excitation, and φ denotes the phase angle.

Figure 5(b) compares the dynamic stiffness and damping of different yaw dampers at the displacement amplitude of 1 mm. The FSS damper demonstrates a significant increase in the dynamic stiffness until it reaches saturation near 5 Hz. Its dynamic stiffness is close to that of YD1 at a low frequency of 1 Hz but approximates to that of YD2 at higher frequencies. To quantify the frequency-dependent stiffness characteristic, we define an index R_K as the ratio of the dynamic stiffness at 10 Hz to one at 1 Hz. R_K corresponding to YD1 and YD2 is 2.37 and 2.19, respectively, while that for the FSS damper is 4.49. Hence, the FSS damper exhibits more significant frequency-dependent stiffness, which is exactly its most remarkable characteristic different from conventional dampers. Additionally, the dynamic damping of the FSS damper is the smallest at low frequencies and becomes moderate with further increasing excitation frequency.

The comparison of the dynamic characteristics at the displacement amplitude of 2 mm is shown in Figure 5(c). It can be observed that the FSS damper provides a moderate dynamic stiffness at frequencies below 3 Hz while a stiffness very close to that of YD2 at higher frequencies. The similar features are also observed concerning the dynamic damping. Overall, the stiffness variation of the FSS damper is more significant. Its corresponding R_K is 2.18, while that for YD1 and YD2 is 1.79 and 1.23, respectively.

In summary, a noticeable feature of the FSS damper is that its dynamic stiffness varies significantly with excitation frequency, exhibiting a lower stiffness at low frequencies and a higher stiffness at high frequencies. According to the sensitivity analysis in Section 2.3, this feature is conducive to ensuring the vehicle stability during long-term operation, under complicated wheel-rail contact geometries. However, the dynamic stiffness of YD1 remains at a low level regardless of excitation frequency, while that of YD2 is high even at a low frequency. Previous operational experience has indicated that the former usually results in high-frequency bogie hunting in the late stage of a wheel reprofiling cycle, and conversely, the latter tends to cause low-frequency carbody hunting under the new wheel condition [34].

3.2. Numerical modelling of the yaw damper

It is necessary to establish an accurate numerical model of the yaw damper for vehicle dynamics analysis. Although the physical model [37,38] has the advantage of accurately reproducing the damper's behaviour by modelling the pressure-flow relationship between relevant critical components, it is unsuitable for numerical simulations of vehicle dynamics due to its high computational burden and many inaccessible input parameters. In contrast, as an equivalent parameter model, the Maxwell model has been widely used for vehicle dynamics simulations [39]. Typically, the dashpot in the Maxwell model is considered nonlinear and adopts the static characteristic curve of the damper, whereas the series stiffness is usually treated as a constant. This treatment can only account for the dynamic characteristics at specific excitation frequencies and amplitudes. It has been validated that modelling both the spring and dashpot as nonlinear can further improve the model accuracy [40–42]. Accordingly, this paper adopts the Maxwell model with nonlinear spring and dashpot to represent the yaw damper and presents a new parameter tuning procedure based on the test results.

Since the lateral stability of high-speed trains is mainly determined by the dynamic rather than static characteristics of the yaw damper, this study aims to establish the nonlinear Maxwell model to simulate the dynamic behaviour of the FSS yaw damper at small excitation amplitudes of 1 and 2 mm. For the conventional Maxwell model, as shown in Figure 6(a), assume that the excitation displacement x is sinusoidal. The maximum velocity $v_{\max}$ of the input excitation is obtained as:

$$v_{\max} = 2\pi f d_0 \tag{13}$$

Where f is the excitation frequency. According to the vector diagram illustrating the phase shift among the displacement, velocity and force, the maximum velocity $v_{1\max}$ of the series dashpot is

$$v_{1\,\max} = v_{\max} \sin\varphi \tag{14}$$

If the dynamic damping C_{yd} is known, then the force amplitude $F_{d\max}$ of the series dashpot can be written as

$$F_{d\,\max} = v_{1\,\max} C_{\mathrm{yd}} \tag{15}$$

Similarly, the maximum deformation $s_{\max}$ of the series spring is derived as

$$s_{\max} = \max(x - x_1) = d_0 \cos\varphi \tag{16}$$

Moreover, the series spring bears the same force as does the series dashpot, so the output force $F_{s\max}$ of the spring is equal to $F_{d\max}$.

Based on the dynamic characteristic measurements of the yaw damper, the nonlinear force-velocity ($F_{d\max}$-$v_{1\max}$) characteristic of the series dashpot and nonlinear force-displacement ($F_{s\max}$-$s_{\max}$) characteristic of the series spring can be determined in the Maxwell model according to Equations (13)-(16). The nonlinear characteristic curves consist of a set of discrete points, each of which corresponds to one testing condition at a specific frequency and amplitude. In this study, the dynamic characteristic test of the damper considers excitation amplitudes of 1 and 2 mm in the frequency range of 1–10 Hz at intervals of 1 Hz, so 20 discrete points can be obtained for each nonlinear characteristic curve. Moreover, because the numerical simulation will use the interpolation technique, the nonlinear characteristic curves must increase monotonically. Any points violating this principle should be removed. The obtained nonlinear force-velocity and force-displacement characteristics in the Maxwell model are shown in Figure 6(b) as blue lines with plus signs (+). It is not advisable to directly implement them in vehicle dynamics simulations as this would still yield significant simulation errors [41]. Instead, these original nonlinear characteristics of the spring and dashpot can be regarded as crucial foundations for identifying superior alternatives capable of achieving higher simulation accuracy.

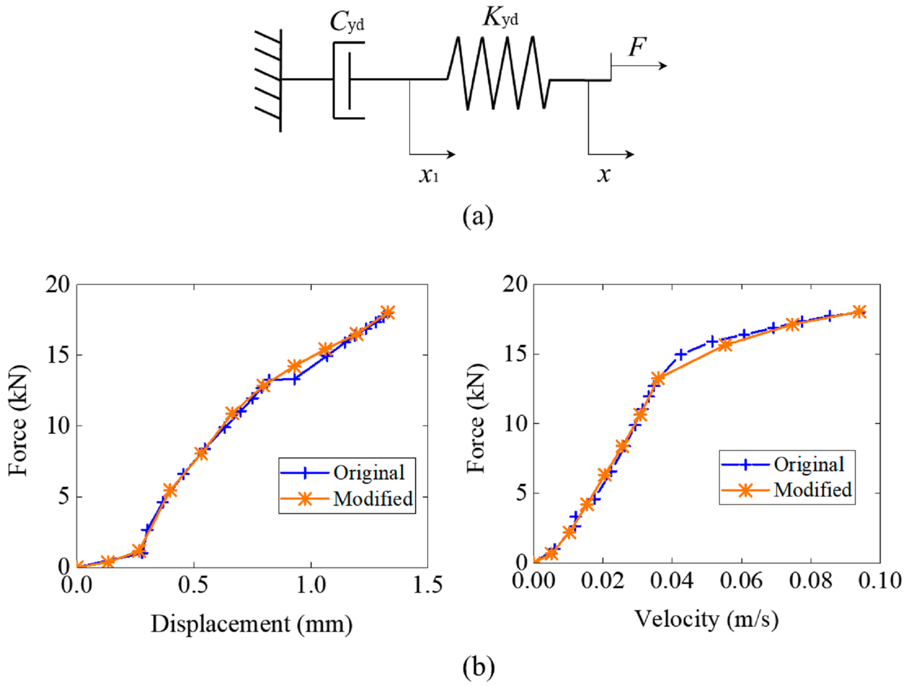

Figure 6. (a) Maxwell model and (b) nonlinear characteristics of the spring and dashpot in the Maxwell model.

Considering the trade-off between model accuracy and parameter tuning difficulty, we assume that the nonlinear force-displacement and force-velocity curves used in vehicle dynamics simulations are symmetrical about the coordinate origin and adopt 10 discrete points to describe the characteristic of each curve in the first quadrant. The optimal nonlinear curves in the Maxwell model are to be realised by an optimisation procedure, before which the displacement and velocity coordinates are determined first. In order to obtain a smooth nonlinear relationship, the discrete point is uniformly distributed along the displacement coordinate. However, since the original nonlinear characteristic curve of the dashpot clearly blows off as the velocity increases, more uniformly distributed points are introduced in low-velocity regions. Then, the 20 force values describing the two nonlinear relationships are considered design variables. The objective function needs to indicate the difference between dynamic characteristic measurements and simulated results, thus being defined as.

$$G(F) = \sum_{i=1}^{N_{d_0}} \sum_{j=1}^{N_f} (w_K e_{Kij}^2 + w_C e_{Cij}^2) \tag{17}$$

$$e_K = \frac{K_{\mathrm{yd}}^{\mathrm{s}} - K_{\mathrm{yd}}^{\mathrm{m}}}{K_{\mathrm{yd}}^{\mathrm{m}}}, \quad e_C = \frac{C_{\mathrm{yd}}^{\mathrm{s}} - C_{\mathrm{yd}}^{\mathrm{m}}}{C_{\mathrm{yd}}^{\mathrm{m}}} \tag{18}$$

where F represents the force values to be determined, N_{d_0} and N_f are the number of amplitudes and frequencies of harmonic excitations, respectively, e_K and e_C refer to the relative

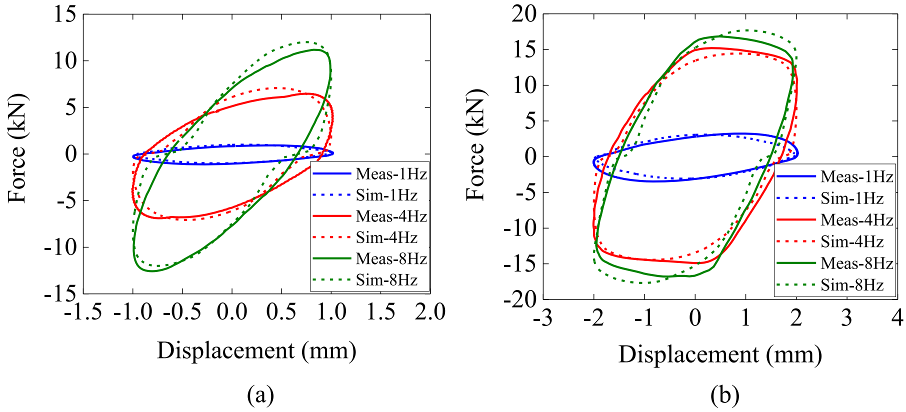

Figure 7. Comparison of the hysteresis curves obtained from the measurements and simulated results: (a) $d_0 = 1$ mm; (b) $d_0 = 2$ mm.

error between measurements (K^{m}_{yd}, C^{m}_{yd}) and simulated results (K^{s}_{yd}, C^{s}_{yd}), and w_K and w_C represent weighting coefficients. In this study, $w_K = 2$ and $w_C = 1$ are used to underline the importance of the dynamic stiffness. The optimisation procedure starts from the force coordinate obtained by performing an interpolation based on the original nonlinear characteristics of the spring and dashpot, making it faster to achieve the optimal solution. The genetic algorithm is used to solve the optimisation problem, and the obtained optimal nonlinear force-displacement and force-velocity relationships are shown in Figure 6(b) as orange lines with asterisks (à). It can be observed that the optimal nonlinear curves to be implemented in numerical simulations make some modifications compared with the original characteristics. Although these modifications are slight, they exert an important influence on the simulated results.

Figure 7 compares the measurements and numerical results obtained from the nonlinear Maxwell model in terms of hysteresis curves. Overall, the simulated results are in good agreement with the measurements. Therefore, the nonlinear Maxwell model obtained by the proposed parameter tuning procedure can effectively reproduce the dynamic behaviour of the yaw damper. Also, it can be found that the simulated hysteresis curves are not as smooth as the test ones, which is attributed to the fact that the dynamic behaviour of the yaw damper is so complex that the nonlinear Maxwell model as a relatively simple model cannot fully capture its characteristics. In fact, the yaw damper experiences stochastic displacement excitations in actual operational scenarios rather than harmonic ones. The nonlinear Maxwell model has also proven to produce numerical forces consistent with experimental ones in actual working conditions [42].

The dynamic stiffness and damping of the yaw damper are further compared between the measurements and simulated results, as shown in Figure 8. It can be seen that the simulated results obtained from the nonlinear Maxwell model match the measurements well at various excitation amplitudes and frequencies. The maximum relative error for the dynamic stiffness is 12.5%, occurring at the amplitude of 1 mm and frequency of 2 Hz, while that for the dynamic damping is 19.4% at the amplitude of 1 mm and frequency of 3 Hz. It can be drawn that the nonlinear Maxwell model can generate satisfactory simulated results and thus is suitable for vehicle dynamics simulations. In addition, in the following

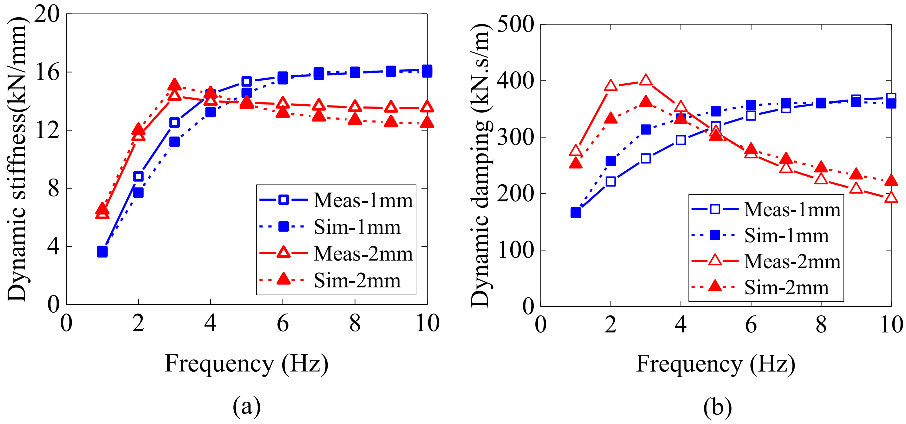

Figure 8. Comparison of the dynamic characteristics from the measurements and simulated results: (a) dynamic stiffness; (b) dynamic damping.

vehicle stability analysis, the nonlinear Maxwell model is also used to simulate the dynamic behaviour of YD1 and YD2 with the calibration data from Ref [34]. It can yield the similar modelling accuracy, and the comparison between the measurements and simulated results is not given for brevity.

4. Lateral stability assessment

This section performs the vehicle dynamics analysis by incorporating the nonlinear Maxwell model of the yaw damper into the multibody vehicle dynamic model. The main parameters of the vehicle model are presented in Appendix. In comparison with the conventional yaw dampers, the improvement of the vehicle dynamics after adopting the FSS damper is assessed with a focus on the lateral stability at extreme wheel-rail contact conicities.

4.1. Carbody stability

Adopting different yaw dampers, Figure 9 illustrates the lateral carbody acceleration under the low-conicity condition defined in Table 1. YD1 can achieve the best carbody stability with the carbody vibration showing a stochastic feature, while YD2 results in the largest lateral carbody acceleration, and hunting instability has arisen. Since the dynamic characteristics of the FSS damper approximate those of the YD1 at lower frequencies, it leads to a similar vibration response of the carbody, which is significantly weaker than that produced by YD2. The carbody vibration energy is concentrated in the frequency range of 1–2 Hz. The vehicle equipped with YD2 demonstrates an obvious dominant frequency of 1.4 Hz, at which the acceleration amplitude is significantly larger than that produced by YD1 and FSS damper. The lateral ride comfort indexes corresponding to YD1, YD2, and FSS damper are 2.3, 2.61, and 2.37, respectively. As YD2 fails to ensure the ride comfort within the excellent level, it is unacceptable to adopt it if the vehicle experiences a low equivalent conicity.

Besides the wheel-rail contact conicity, the running speed and wheel-rail friction coefficient also have a significant impact on carbody hunting [43]. To acquire a comprehensive

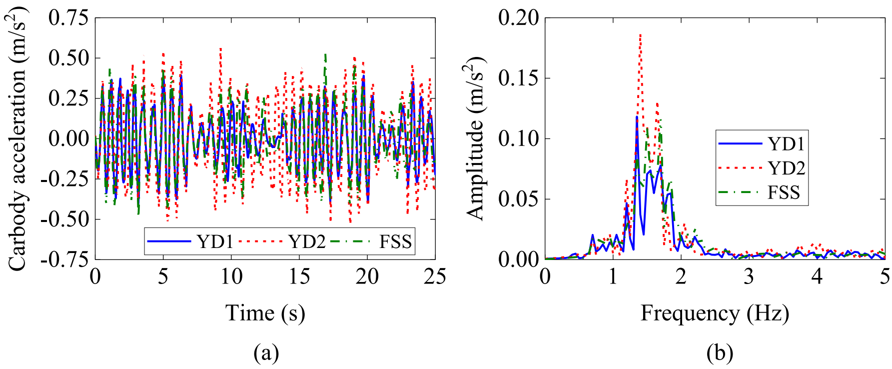

Figure 9. Comparison of the lateral carbody acceleration at low conicity: (a) results in the time domain; (b) results in the frequency domain.

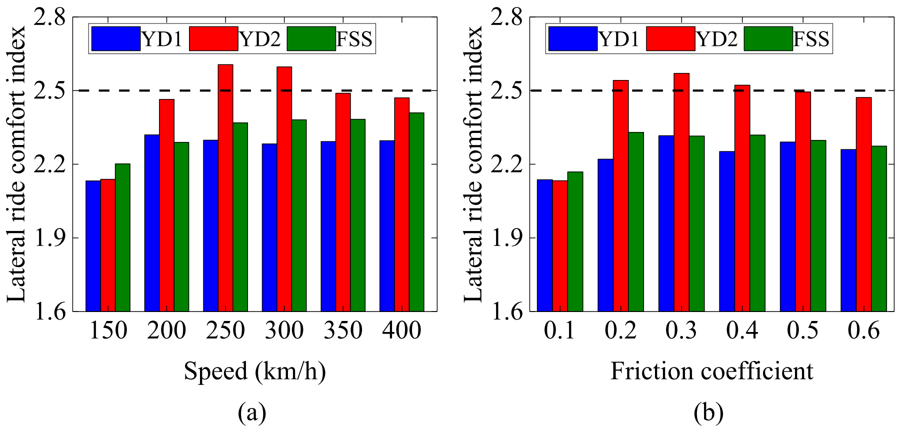

Figure 10. Comparison of the lateral ride comfort index with varying (a) speed and (b) wheel-rail friction coefficient

understanding of the effect of different yaw dampers on carbody stability, the comparison of the lateral ride comfort at low conicity considers the variations in these factors, as presented in Figure 10.

The ride comfort index of the vehicle equipped with YD2 is sensitive to the running speed. As the speed increases, the ride comfort index first increases and then decreases. The value of the ride comfort index has exceeded 2.5 when the speed is 250–300 km/h. On the contrary, after the speed exceeds 150 km/h, the ride comfort index achieved by YD1 and FSS damper changes slightly and is below 2.5, indicating favourable carbody stability under variable-speed conditions.

The wheel-rail friction coefficient also significantly influences the lateral ride comfort. All three different yaw dampers can achieve excellent ride comfort with a friction coefficient of 0.1. Nevertheless, once the friction coefficient is higher than 0.1, the ride comfort of the vehicle adopting YD2 will significantly deteriorate, resulting in a ride comfort index higher than 2.5 when the friction coefficient ranges from 0.2–0.4. The ride comfort of the vehicle adopting YD1 and FSS damper is less sensitive to the friction coefficient. Their corresponding indexes also increase as the friction coefficient exceeds 0.1 but are well below the limit value.

The above results indicate that adopting YD2 is prone to give rise to carbody hunting at low conicity due to its high dynamic stiffness, especially considering the varied operational scenarios of the vehicle. Conversely, since YD1 and FSS damper have a reduced stiffness at lower frequencies, they can improve the vehicle's adaptability and ensure the carbody stability at low conicity.

4.2. Bogie stability

The bogie stability of the vehicle adopting different yaw dampers is compared in Figure 11 under the high-conicity condition defined in Table 1. Figure 11(a) illustrates the sliding RMS of bandpass-filtered lateral bogie frame acceleration. It can be observed that YD1 results in more severe bogie frame vibrations over the whole travel distance. The global maximum of the moving RMS occurs around the 300 m position marker, and the corresponding values for YD1, YD2, and FSS damper are 4.14, 2.06, and 2.58 m/s^2, respectively. Figure 11(b) displays a section of related filtered bogie fame acceleration in the time domain. When using YD1, the vehicle exhibits a significantly higher acceleration amplitude, which can be explained by the frequency spectrum shown in Figure 11(c). It is seen that YD1 results in more bogie frame vibration energy concentrated in the frequency range of 5–9 Hz, whereas YD2 and FSS damper effectively suppress the vibration energy by enhancing the kinematic restriction between the bogie frame and carbody through their high stiffness.

The bogie stability of the vehicle is further investigated through the bifurcation diagram of the lateral wheelset displacement depending on the running speed, as shown in Figure 12. Besides the high-conicity condition, the bifurcation analysis also considers the normal-conicity condition with the standard wheel-rail profile combination. The brute-force method [44] is used here to obtain the bifurcation diagram. It requires a set of numerical simulations, in which the wheelset oscillation occurs as a result of a lateral disturbance, and the simulation continues on an ideal track. Then, the stationary solution and amplitude of the limit cycle are identified when the attractor is reached.

The wheelset behaviour demonstrates a typical supercritical Hopf bifurcation under both normal and high conicity conditions no matter which type of yaw damper is adopted. The amplitude of the wheelset oscillation starts from zero and increases gradually with vehicle speed. In this study, the vehicle is regarded as unstable once the oscillation amplitude increases beyond 0.5 mm, and the nonlinear critical speed is determined accordingly. Adopting YD2 offers the vehicle a high critical speed, with 670 km/h at normal conicity and 550 km/h at high conicity. In contrast, the FSS damper results in the lowest critical speed of the vehicle under both conicity conditions. It is about 410 km/h at normal conicity and 360 km/h at high conicity. However, the limit cycle amplitude develops slowly with the FSS damper adopted. Under the normal-conicity condition, the FSS damper leads to a smaller limit cycle amplitude compared with YD1 when the running speed exceeds 490 km/h. This feature also can be observed under the high-conicity condition when the vehicle speed exceeds 370 km/h. Actually, when the wheelset runs with a small-amplitude limit cycle motion, the limit value of the practical assessment quantity applied in vehicle acceptance

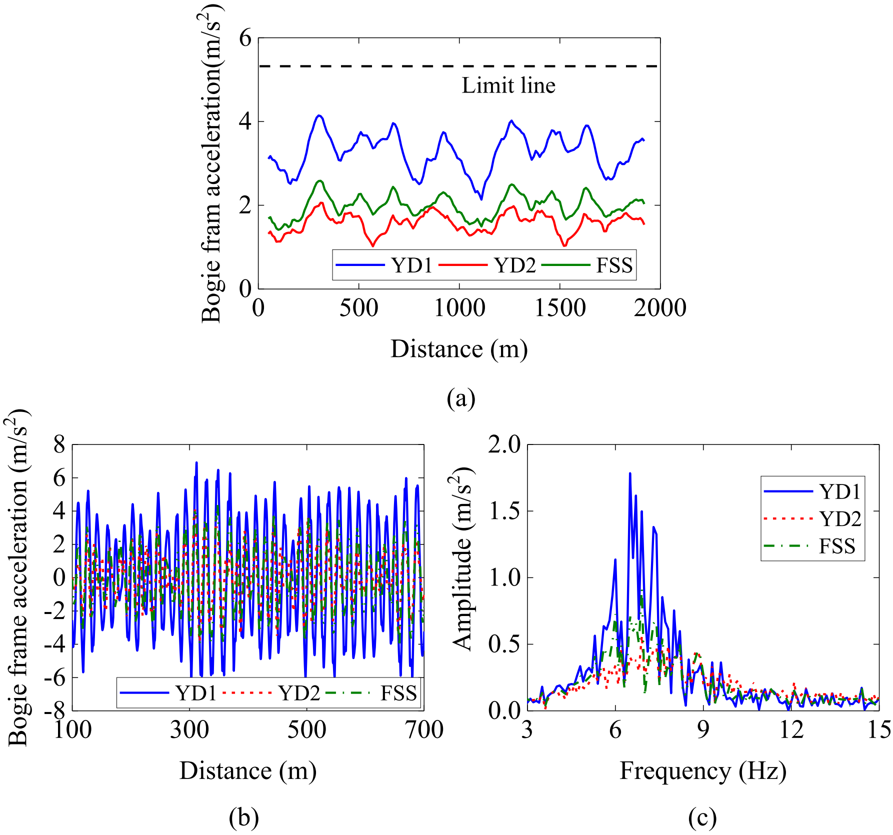

Figure 11. Comparison of the lateral bogie frame acceleration at high conicity: (a) sliding RMS of bandpass-filtered bogie frame acceleration; (b) filtered bogie frame acceleration in the time domain; (c) bogie frame acceleration in the frequency domain.

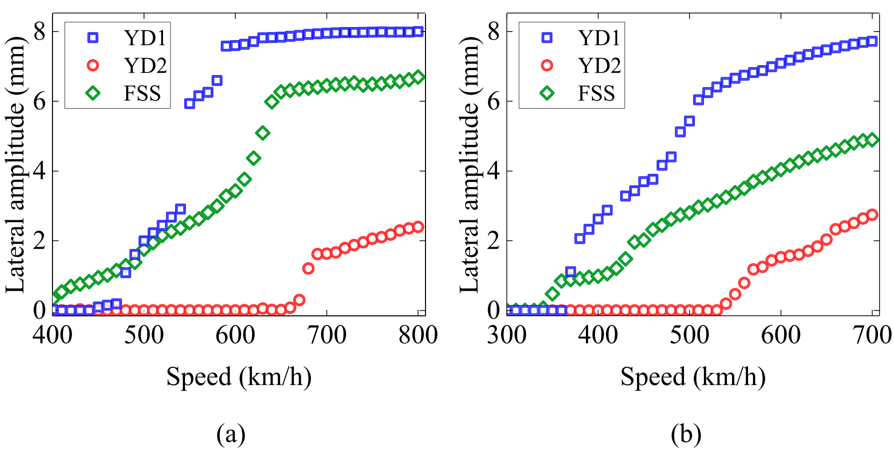

Figure 12. Bifurcation diagrams of the wheelset lateral displacement at (a) normal conicity and (b) high conicity.

regulations will often not be achieved [45]. Furthermore, the wheelset motion with a small-amplitude limit cycle can properly broaden the wheel-rail contact bandwidth, effectively suppressing the formation of severe wheel hollow wear [46]. Therefore, even though the FSS damper yields a limit cycle motion of the wheelset at a relatively low speed, it does not necessarily mean a detrimental effect on the running dynamics of the vehicle.

The nonlinear critical speed is also evaluated from the perspective of the bogie frame acceleration. For the intuitive comparison, the maximum value of the sliding RMS of bandpass-filtered lateral bogie frame acceleration is normalised with respect to the limit value defined in Equation (2), as shown in Figure 13. The acceleration-based method delivers a significantly higher critical speed than the results obtained by the bifurcation diagram method. The vehicle equipped with YD1 first reaches the limit value with the increase of running speed, leading to a critical speed of 580 km/h at normal conicity and 460 km/h at high conicity. On the contrary, YD2 realises a large stability margin of the vehicle, whose bogie frame acceleration is well below the limit value within the investigated speed range. It is important to note that although the FSS damper results in the lowest critical speed in the bifurcation analysis, it achieves excellent running stability of the vehicle according to the acceleration-based method. Under the normal-conicity condition, the FSS damper keeps the bogie frame acceleration between those achieved by YD1 and YD2, and the vehicle remains stable when the speed has reached 700 km/h. Under the high-conicity condition, the FSS damper leads to the running stability similar to that obtained by using YD2, achieving a critical speed higher than 600 km/h. Additionally, by comparing the results in Figures 12 and 13, it can be drawn that if the limit cycle amplitude is sufficiently large, the bogie frame acceleration will exceed the limit value.

In summary, YD1 and YD2 have a distinct effect on the vehicle stability. Specifically, adopting YD1 is beneficial to carbody stability at low conicity due to its low dynamic stiffness, whereas this would worsen bogie stability at high conicity and yield severe lateral bogie frame vibrations. On the contrary, with a high dynamic stiffness over the frequency range of interest, YD2 achieves excellent bogie stability but gives rise to carbody hunting. As a new smart passive damper, the FSS yaw damper exhibits significant frequency-dependent dynamic stiffness, with a low value at low frequencies and a high value at high frequencies. As a result, it combines the advantages of both conventional yaw dampers and can ensure the vehicle stability under complicated wheel-rail contact geometries. This would lower the requirements for wheel reprofiling and rail grinding and thus reduce the costs in operation and maintenance of wheel-rail systems.

5. Conclusions

Based on the sensitivity analysis of the stability of a high-speed railway vehicle, this study presents an innovative passive yaw damper, namely the frequency-selective stiffness (FSS) damper, to improve the vehicle stability at extreme wheel-rail contact conicities. The static and dynamic characteristics of the FSS damper are obtained through a series of experimental tests and then compared with those of two types of conventional passive dampers. To examine the effect of the FSS damper on the vehicle dynamic performance, we propose a parameter determination procedure for the nonlinear Maxwell model to emphatically simulate the dynamic behaviour of the yaw damper. The following conclusions can be drawn:

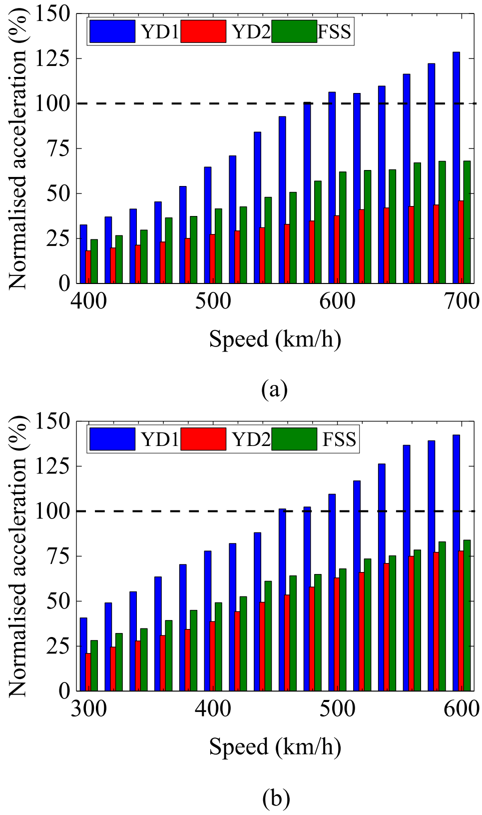

Figure 13. Normalised lateral bogie frame acceleration at (a) normal conicity and (b) high conicity

(1) The sensitivity analysis indicates that the dynamic stiffness of the yaw damper has the most significant influence on the vehicle stability among several crucial suspension parameters. The vehicle stability has distinct requirements for the stiffness value considering different wheel-rail contact conicities. A low stiffness is beneficial to carbody stability at low wheel-rail contact conicity, while a high stiffness contributes to bogie stability at high conicity.

(2) No special features are observed regarding the static characteristics of the FSS damper compared with conventional dampers. However, its dynamic stiffness exhibits more significant frequency-dependent characteristics, showing a lower value at low frequencies and a higher value at high frequencies. The simulated results of the presented nonlinear Maxwell model can accurately capture such dynamic behaviour of the FSS damper and show good agreement with the test results. This model is suitable for vehicle dynamics simulations due to its high computational efficiency.

(3) Currently adopted conventional yaw dampers fail to achieve favourable vehicle stability at varied conicity due to their limited ability to obtain frequency-dependent stiffness. In contrast, the FSS damper can ensure excellent carbody stability and bogie stability under extreme conicity conditions. The resulting lateral ride comfort of the vehicle at low conicity remains within the excellent level, even considering

variations in running speed and wheel-rail friction coefficient. In addition, the vehicle equipped with the FSS damper demonstrates a supercritical Hopf bifurcation at normal and high conicities, with the slow development of limit cycle amplitudes. According to the assessment of lateral bogie frame acceleration, the bogie stability at both conicities has an adequate safety margin when the vehicle operates at high speeds.

Disclosure statement

No potential conflict of interest was reported by the author(s).

Funding

The material in this paper is based on work supported by the National Natural Science Foundation of China [grant numbers 52372403; U2268211], the Natural Science Foundation of Sichuan Province [grant number 2022NSFSC0034], and the National Railway Group Science and Technology Program [grant number N2023J071].

ORCID

Yuan Yao http://orcid.org/0000-0003-2279-7463

References

[1] Sun JF, Chi MR, Jin XS, et al. Experimental and numerical study on carbody hunting of electric locomotive induced by low wheel-rail contact conicity. Veh Syst Dyn. 2021;59(2):203–223. doi:10.1080/00423114.2019.1674344
[2] Li YX, Chi MR, Guo ZT, et al. An abnormal carbody swaying of intercity EMU train caused by low wheel–rail equivalent conicity and damping force unloading of yaw damper. Rail Eng Sci. 2023;31(3):252–268. doi:10.1007/s40534-022-00295-w
[3] Shi HL, Wang JB, Wu PB, et al. Field measurements of the evolution of wheel wear and vehicle dynamics for high-speed trains. Veh Syst Dyn. 2018;56(8):1187–1206. doi:10.1080/00423114.2017.1406963
[4] Yi YS, Dai HY, Qi YY, et al. Experimental study of bogie instability monitoring and suppression measures for high-speed EMUs. Proc Inst Mech Eng Part F-J Rail Rapid Transit. 2023;237(10):1260–1272. doi:10.1177/09544097231160362
[5] Steyn E, Paulsson B, Ekberg A, et al. Rail machining - current practices and potential for optimization. Proc Inst Mech Eng Part F-J Rail Rapid Transit. 2024;238(2):196–205. doi:10.1177/09544097231187978
[6] Mousavi Bideleh SM, Berbyuk V, Persson R. Wear/comfort pareto optimisation of bogie suspension. Veh Syst Dyn. 2016;54(8):1053–1076. doi:10.1080/00423114.2016.1180405
[7] Yao Y, Li G, Wu GS, et al. Suspension parameters optimum of high-speed train bogie for hunting stability robustness. Int J Rail Transp. 2020;8(3):195–214. doi:10.1080/23248378.2019.1625824
[8] Li G, Wu RD, Deng XX, et al. Suspension parameters matching of high-speed locomotive based on stability/comfort pareto optimization. Veh Syst Dyn. 2022;60(11):3848–3867. doi:10.1080/00423114.2021.1979602
[9] Chen XW, Shen LJ, Hu XY, et al. Suspension parameter optimal design to enhance stability and wheel wear in high-speed trains. Veh Syst Dyn. 2024;62(5):1230–1252. doi:10.1080/00423114.2023.2224905
[10] Guo ZT, Chi MR, Sun JF, et al. Experimental and numerical research on the bogie hunting of a high-speed train caused by the empty stroke of yaw damper. Veh Syst Dyn. 2023; doi:10.1080/00423114.2023.2250887

[11] Jiang CC, Zhang H, Ling L, et al. The effect of yaw damper performance degradation on carbody hunting of high-speed trains. Veh Syst Dyn. 2024;33; doi:10.1080/00423114.2024.2317397
[12] Alonso A, Gimenez JG, Gomez E. Yaw damper modelling and its influence on railway dynamic stability. Veh Syst Dyn. 2011;49(9):1367–1387. doi:10.1080/00423114.2010.515031
[13] Xia ZH, Zhou JS, Gong D, et al. Theoretical study on the effect of the anti-yaw damper for rail vehicles. Proc Inst Mech Eng Part F-J Rail Rapid Transit. 2020;234(2):457–473.
[14] Yan Y, Zeng J, Huang CH, et al. Bifurcation analysis of railway bogie with yaw damper. Arch Appl Mech. 2019;89:1185–1199. doi:10.1007/s00419-018-1475-6
[15] Bustos A, Tomas-Rodriguez M, Rubio H, et al. On the nonlinear hunting stability of a high-speed train bogie. Nonlinear Dyn. 2023;111(3):2059–2078. doi:10.1007/s11071-022-07937-y
[16] Li G, Yao Y, Shen LJ, et al. Influence of yaw damper layouts on locomotive lateral dynamics performance: pareto optimization and parameter analysis. J Zhejiang Univ-SCI A. 2023;24(5):450–464. doi:10.1631/jzus.A2200374
[17] Diana G, Bruni S, Cheli F, et al. Active control of the running behaviour of a railway vehicle: stability and curving performances. Veh Syst Dyn. 2002;37(sup1):157–170. doi:10.1080/00423114.2002.11666229
[18] Braghin F, Bruni S, Resta F. Active yaw damper for the improvement of railway vehicle stability and curving performances: simulations and experimental results. Veh Syst Dyn. 2006;44(11):857–869. doi:10.1080/00423110600733972
[19] Alfi S, Bruni S, Goodall RM, et al. Secondary yaw control to improve curving vs. stability trade-off for a railway vehicle. Veh Syst Dyn. 2023;61(5):1367–1386. doi:10.1080/00423114.2022.2094277
[20] Shi HL, Zeng J, Qu S. Linear stability analysis of a high-speed rail vehicle concerning suspension parameters variation and active control. Veh Syst Dyn. 2023;61(11):2976–2998. doi:10.1080/00423114.2022.2147086
[21] Guo JY, Shi HL, Zeng J. Bifurcation and stability analysis of a high-speed rail vehicle with active yaw dampers. J Vib Control. 2023; doi:10.1177/10775463231196272
[22] Wang X, Liu BB, Di Gialleonardo E, et al. Application of semi-active yaw dampers for the improvement of the stability of high-speed rail vehicles: mathematical models and numerical simulation. Veh Syst Dyn. 2022;60(8):2608–2635. doi:10.1080/00423114.2021.1912366
[23] Zhang XX, Li H, Cheng J, et al. Adaptive stability mechanism of high-speed train employing parallel inerter yaw damper. Veh Syst Dyn. 2023;61(1):38–57. doi:10.1080/00423114.2022.2045027
[24] Isacchi G, Ripamonti F, Corsi M, et al. A smart passive yaw damper for the reduction of lateral contact forces in low-radius curved tracks. 15th world congress on computational mechanics (WCCM-XV), Yokohama, Japan, July 2022.
[25] Isacchi G, Ripamonti F, Corsi M. Innovative passive yaw damper to increase the stability and curve-taking performance of high-speed railway vehicles. Veh Syst Dyn. 2023;61(9):2273–2291. doi:10.1080/00423114.2022.2105242
[26] Li G, Zhou Y, Yao Y, et al. Application of yaw dampers with frequency-selective damping to improve the locomotive adaptability to low/high conicity stability. Proc Inst Mech Eng Part F-J Rail Rapid Transit. 2023;237(6):784–795. doi:10.1177/09544097221141517
[27] Yao Y, Chen XW, Li H, et al. Suspension parameters design for robust and adaptive lateral stability of high-speed train. Veh Syst Dyn. 2023;61(4):943–967. doi:10.1080/00423114.2022.2062012
[28] Huo WB, Yue BS, Liu XG, et al. The development of stiffness-adjustable anti-yaw damper). 26th symposium of the international association of vehicle system dynamics (IAVSD), Gothenburg, Sweden, August 2019.
[29] GB/T 5599-2019. Specification for dynamic performance assessment and testing verification of rolling stock. Beijing, People's Republic of China: National Railway Administration; 2019.
[30] EN 14363:2016 + A1. - Railway applications - Testing and simulation for the acceptance of running characteristics of railway vehicles - Running behaviour and stationary tests. Brussels: CEN; 2016.

[31] Funfschilling C, Perrin G. Uncertainty quantification in vehicle dynamics. Veh Syst Dyn. 2019;57(7):1062–1086. doi:10.1080/00423114.2019.1601745
[32] Sobol IM. Global sensitivity indices for nonlinear mathematical models and their monte carlo estimates. Math Comput Simul. 2001;55(1-3):271–280. doi:10.1016/S0378-4754(00)00270-6
[33] Vapink V. Statistical learning theory. New York: Wiley; 1998.
[34] Wu HC, Huo WB, Lu Q, et al. Influence study of different anti-yaw dampers on EMUs hunting instability. Electr Drive Locomot. 2017;5:30–34. [In Chinese].
[35] Huang CH, Zeng J. Dynamic behaviour of a high-speed train hydraulic yaw damper. Veh Syst Dyn. 2018;56(12):1922–1944. doi:10.1080/00423114.2018.1439588
[36] EN 13802:2013. Railway applications - suspension components - hydraulic dampers. Brussels: CEN; 2013.
[37] Wang WL, Zhou ZR, Yu DS, et al. Rail vehicle dynamic response to a nonlinear physical 'in-service' model of its secondary suspension hydraulic dampers. Mech Syst Signal Proc. 2017;95:138–157. doi:10.1016/j.ymssp.2017.03.031
[38] Gao HX, Chi MR, Dai LC, et al. Mathematical modelling and computational simulation of the hydraulic damper during the orifice-working stage for railway vehicles. Math Probl Eng. 2020;11:1–23.
[39] Bruni S, Vinolas J, Berg M, et al. Modelling of suspension components in a rail vehicle dynamics context. Veh Syst Dyn. 2011;49:1021–1072. doi:10.1080/00423114.2011.586430
[40] Mellado AC, Vinolas J, Gomez E. Advances on railway yaw damper characterization exposed to small displacements. Int J Heavy Veh Syst. 2006;13(4):263–280. doi:10.1504/IJHVS.2006.010583
[41] Teng WX, Shi HL, Luo R, et al. Improved nonlinear model of a yaw damper for simulating the dynamics of a high-speed train. Proc Inst Mech Eng F-J Rail Rapid Transit. 2018;233(7):651–665. doi:10.1177/0954409718804414
[42] Isacchi G, Ripamonti F, Corsi M. A meta-heuristic optimization procedure for the identification of the nonlinear model parameters of hydraulic dampers based on experimental dataset of real working conditions. J Comput Nonlinear Dyn. 2023;18(9):091004, doi:10.1115/1.4062541
[43] Luo R, Teng WX, Wu XW, et al. Dynamics simulation of a high-speed railway car operating in low-temperature environments with stochastic parameters. Veh Syst Dyn. 2020;58(12):1914–1934. doi:10.1080/00423114.2019.1662922
[44] Polach O, Kaiser I. Comparison of methods analyzing bifurcation and hunting of complex rail vehicle models. J Comput Nonlinear Dyn. 2012;7(4):041005, doi:10.1115/1.4006825
[45] Polach O. On non-linear methods of bogie stability assessment using computer simulations. Proc Inst Mech Eng Part F-J Rail Rapid Transit. 2006;220:13–27. doi:10.1243/095440905X33251
[46] Zhai WM, Jin XS, Wen ZF, et al. Wear problems of high-speed wheel/rail systems: observations, causes, and countermeasures in China. Appl Mech Rev. 2020;72(6):060801, doi:10.1115/1.4048897

Appendix

Table A1. Main parameters of the high-speed train.

Parameter	Value	Unit
Carbody mass	35940	kg
Bogie frame mass	2200	kg
wheelset mass	1520	kg
Carbody roll moment of inertia	96.1	$t{\cdot}m^2$
Carbody pitch moment of inertia	1700	$t{\cdot}m^2$
Carbody yaw moment of inertia	1670	$t{\cdot}m^2$
Bogie frame roll moment of inertia	1236	$kg{\cdot}m^2$
Bogie frame pitch moment of inertia	1233	$kg{\cdot}m^2$
Bogie frame yaw moment of inertia	2336	$kg{\cdot}m^2$
Wheelset roll moment of inertia	693	$kg{\cdot}m^2$
Wheelset pitch moment of inertia	118	$kg{\cdot}m^2$
Wheelset yaw moment of inertia	693	$kg{\cdot}m^2$
Primary longitudinal stiffness	40	kN/mm
Primary lateral stiffness	12.5	kN/mm
Primary vertical damping	10	kN·s/m
Secondary longitudinal stiffness	0.133	kN/mm
Secondary lateral stiffness	0.133	kN/mm
Secondary vertical stiffness	0.203	kN/mm
Secondary lateral damping	15	kN·s/m
Stiffness of anti-roll bar	4.15	MN.m/rad
Wheel base	2.5	m
Distance between bogie centres	17.38	m
Wheel rolling radius	0.46	m